Highly Conductive CdS Inverse Opals for Photochemical Solar Cells

*Tao Ling, Sergei A. Kulinich, Zi-Ling Zhu, Shi-Zhang Qiao, and Xi-Wen Du**

Semiconductor materials with an inverse opal structure have previously demonstrated promise for photovoltaic applications. However, their use in solar cells is still restricted by their poor electron transfer properties. Here, highly conductive CdS inverse opal structures are prepared via a multistep process, where CdS inverse opal backbones are first built up on conductive glass substrates via co-deposition of CdS quantum dots and polystyrene microspheres, followed by calcination, after which subsequent electrodepositon and annealing treatments are applied to transform the fine constituent nanocrystals into larger ones, thus considerably enhancing the electrical conductivity. The obtained CdS networks are tested as anodes in photochemical solar cells and demonstrate conversion efficiency values up to 2.00% under the illumination of one sun. After depositing an additional CdSe layer, the conversion efficiency of the structures is further increased to 2.47%.

1. Introduction

Various nanostructured materials have already shown promise for reducing the cost and improving the efficiency of solar cells (SCs).[1–7] The nanostructures commonly used for photovoltaic applications include nanocrystals (quantum dots), nanorods and nanowires,[1,2,4] which exhibit adjustable band gaps,[2,8,9] carrier multiplication[10–13] and low-temperature solution processing.[1,2,4] Recently, more complex 3D nanostructures, such as nanowire arrays,[14] have been theoretically and experimentally demonstrated to be more efficient in improving light absorption and charge separation and collection,[3,7] especially when the electrode thickness is comparable to the optical absorption length and the lifetime of minority carriers is relatively short.[14]

Dr. T. Ling, Z.-L. Zhu, Prof. S.-Z. Qiao, Prof. X.-W. Du
Tianjin Key Laboratory of Composite and Functional Materials
School of Materials Science and Engineering
Tianjin University
Tianjin, 300072, China
E-mail: xwdu@tju.edu.cn
Dr. S. A. Kulinich
Institute of Innovative Science and Technology
Tokai University
Hiratsuka, Kanagawa, 259-1292, Japan
Prof. S.-Z. Qiao
School of Chemical Engineering
The University of Adelaide
Adelaide, SA5005, Australia

DOI: 10.1002/adfm.201300734

Inverse opal is a well-known 3D structure with highly periodic and uniform pores surrounded by solid walls.[15–19] Such porous walls can provide a prodigious surface area for charge separation,[20] while the periodic structure was demonstrated to enhance remarkably light harvesting efficiency due to photonic or backscattering effects.[21] Recently, TiO_2 inverse opals have been reported to show promise in dye-sensitized[20–26] and semiconductor-sensitized SCs.[27] However, the reported 3D-TiO_2 based SCs suffered from relatively poor electron transport and exhibited low overall efficiencies resulted from numerous interfaces and unreliable electrical contacts inside their porous walls.[20,28,29] Therefore, further development of inverse-opal based SCs heavily depends on the improvement of electron transfer properties of such 3D structures.

Thus far, little work was carried out to improve the electrical conductivity of inverse opal structures.[28–31] Subban et al.[30] and Choi et al.[31] reported the doping of TiO_2 inverse opals with W and Ta, respectively. More recently, Zhang and Braun constructed Ni inverse opals and then coated with Si, thus aiming to achieve a highly conductive anode for Li ion cells.[29] However, the above approaches are not feasible for inverse opal electrodes to be applied in SCs. While low dopant concentrations cannot provide satisfactory conductivity levels, heavy doping may cause a severe recombination of photo-generated carriers. At the same time, the use of metal frameworks will limit the incoming light harvesting, thus decreasing the light collection efficiecy. Therefore, the development of novel effective approaches, aiming at overcoming the poor conductivity of inverse opal nanostructures remains a big challenge.

Cadmium sulfide (CdS) is an important optoelectronic material which has been extensively applied in solar energy conversion applications as a photocatalyst for water-splitting,[32] a sensitizer for photo-electrochemical cells[33] or a window layer in thin-film CdS/CdTe SCs.[34] Many efforts have been made to prepare various CdS nanostructures, such as nanotips,[35] nanowires[14] and nanotubes,[36] aiming to enhance both charge separation and transport. In addition, 3D CdS inverse opals were fabricated by electrochemical deposition[37–39] and chemical bath deposition.[40,41] These works focused on the synthesis and optical application of the CdS inverse opal structure, and highly conductive 3D CdS networks have never been achieved and used in SCs thus far.

The pioneering work of Goldstein et al. demonstrated that the melting temperature of small CdS nanocrystals could be significantly reduced.[42] Hence we propose that highly conductive 3D CdS networks can be first prepared from ultrafine CdS nanocrystals (as building blocks) and then annealed at a low temperature to improve their crystallinity and reduce defect density. In the present work, 3D CdS networks composed of ultrafine CdS nanocrystals (~2 nm) were first built up on conductive glass substrates via a template process.[43] Then, subsequent electrodepositon (ED) and annealing treatments were applied to transform the fine nanocrystals into larger ones, thus considerably enhancing the electrical conductivity of the 3D structures. The obtained CdS networks were tested as anodes in photochemical SCs under the illumination of one sun and demonstrated conversion efficiency values up to 2.00%, which is explained by their efficient light absorption and superior conductivity. To our best knowledge, this is the highest value reported for a liquid-junction SC based on pure CdS nanocrystals and measured by a two-electrode system. After depositing an additional CdSe layer, the conversion efficiency of the structures was further increased to 2.47%.

2. Results and Discussion

The preparation procedures used in this study are briefly shown in **Scheme 1**. First, a conductive glass substrate was inserted vertically into distilled water containing CdS quantum dots (QDs) with an average size of 2 nm and colloidal polystyrene (PS) microspheres of 300 nm in size. The two components deposited simultaneously at the substrate-water-air interface which moved downward with continuous evaporation of the liquid. As a result, a CdS/PS composite film formed on the substrate (see Scheme 1a). The thickness of the prepared inverse opal layer could be well controlled by adjusting the amounts of PS spheres and CdS QDs as shown in Supporting Information Figure S1. An optimum thickness of 2.6 μm was determined by comparing the photovoltaic performance of samples with different thicknesses (Figure S1 and Table S1), after which all further manipulations and post-deposition treatments were performed with 2.6-μm thick structures.

As a second step (Scheme 1b), the PS templates were removed via calcination in air at 400 °C for 1 h to yield an inverse opal structure composed of ultra-fine CdS nanocrystals (hereafter, referred to as the 'as-calcinated structure'). Then, an additional CdS layer was electrodeposited onto the as-calcinated structure (Scheme 1c). The ED stage was very important to thicken and reinforce the walls of the inverse opal structure. On the other hand, as discussed below, it also contributed to a larger grain growth, which in turn ended up in the improved conductivity of the CdS networks. Finally, annealing was conducted to melt small nanocrystals and fuse them together. As a result, the fully-processed structure had larger grains and therefore provided an enhanced electrical conductivity through the entire CdS network (Scheme 1d).

Figure 1a is a typical scanning electron microscope (SEM) image of an as-calcinated structure (Scheme 1b) where a well ordered hexagonal inverse opal network with spherical voids and a wall thickness of 17 nm is seen. More detailed characterization indicated that the walls consisted of fine CdS nanocrystals (Figure S4). A side view SEM image (Figure S1) indicates that the walls of the network are well interconnected and contact directly with the conductive substrate. This is believed to provide a direct and reliable pathway for charge transportation, which is essential for solar conversion. The wall thickness

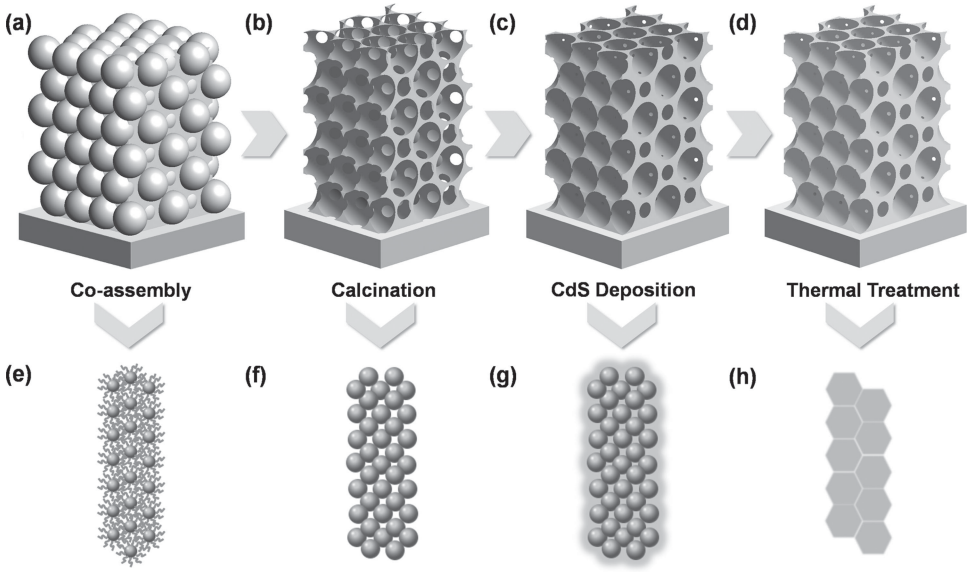

Scheme 1. Schematic illustration of the general fabrication strategy used in this study to prepare highly conductive 3D networks. (a) PS colloidal spheres and CdS QDs are co-assembled on a conductive glass substrate. (b) The sample is calcinated to yield an as-calcinated CdS inverse opal structure. (c) Additional CdS is electrodeposited into the nanopores and on the surface of the as-calcinated CdS network to thicken the walls. (d) Annealing treatment improves the wall crystallinity. (e–h) Microstructural evolution of the CdS networks during stages (a)–(d), respectively. (e) Ligands bound to the QD surfaces. (f) Nanopores form between nanocrystals. (g) Deposited CdS fills in the nanopores. (f) Larger grains constitute the walls.

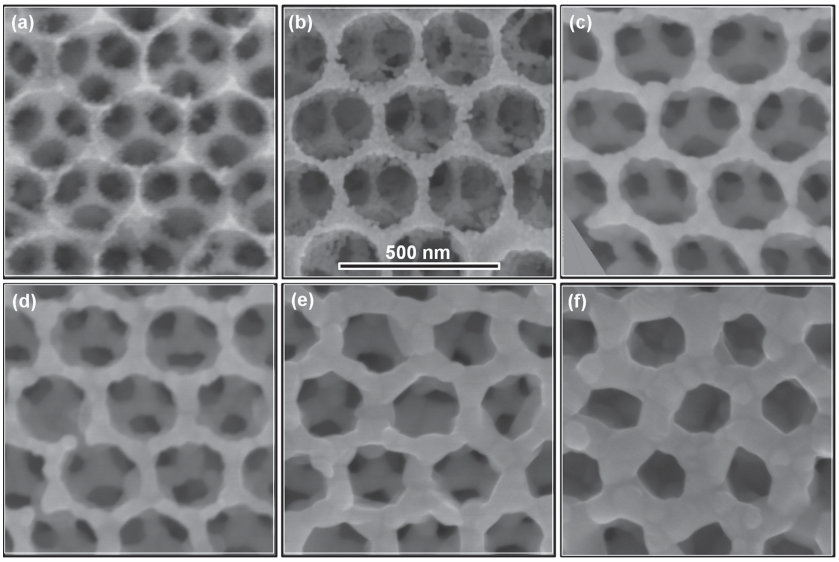

Figure 1. SEM images of (a) as-calcinated 3D CdS structure, (b–f) fully-processed structures after ED of additional CdS layer for 5 (b), 8 (c), 10 (d), 12 (e), and 15 min (f), respectively, and annealing at 400 °C for 1 h. The wall thicknesses in (a–f) are 17, 33, 42, 50, 68, and 85 nm, respectively.

also affects both the light absorption and electron transport properties of the network and can be adjusted by electrodepositing additional CdS layer. As seen in Figure 1b–f, values of about 33, 42, 50, 68, and 85 nm were achieved after electrodepositing additional CdS for 5, 8, 10, 12, and 15 min, respectively.

Transmission electron microscopy (TEM) characterization was carried out to elucidate the sample wall microstructure in greater detail. As seen in **Figure 2**a, the CdS backbone in the as-calcinated structure was porous and built of fine nanocrystals. After 5 min of ED and subsequent annealing, the pores between the nanocrystals were partially filled with CdS (Figure 2b and Figure S5a), while a longer deposition (10 min) resulted in remarkably reduced sizes and number of pores (Figure 2c). Prior to annealing, all structures ED-treated for 5 min or longer demonstrated their constituent CdS nanocrystals to be of about 5 nm in size (Figure S5b). The nanocrystals were observed to fuse, grow bigger and merge together during the subsequent annealing.[42,43] As a result, the walls became very compact and continuous, consisting of larger grains with sizes comparable with the wall thickness (Figure 2d).

Both crystal structure and grain sizes of the as-calcinated and fully-processed samples were evaluated by X-ray diffraction (XRD). As displayed in **Figure 3**, the zinc-blende and wurtzite phases coexisted in the as-calcinated network. Since the wurtzite phase is known to be more stable at temperatures above 300 °C and in crystals bigger than 5 nm,[44,45] it is not surprising that only wurtzite CdS crystals were found in the fully-processed samples. The calculated crystal sizes of the samples presented in Figure 3 are listed in **Table 1**. The average grain size of the as-calcinated inverse opals was very small, 3.5 and 4.3 nm, for the zinc-blende and wurtzite phases, respectively. In the fully-processed samples, this parameter increased considerably with deposition time, reaching ~29 nm after 15 min of ED. The combination of ED and annealing is thus concluded to give rise to networks with both thicker walls and larger grains, which eventually made a remarkable impact on their optical, electronic and photovoltaic properties.

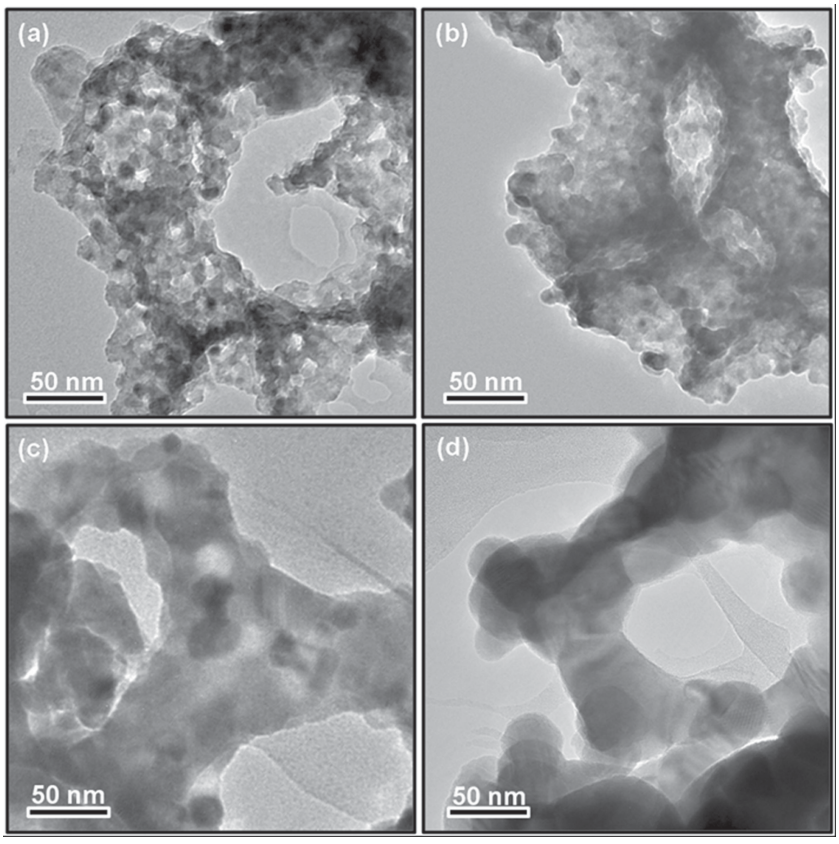

Figure 2. TEM images of (a) as-calcinated CdS inverse opal structure, (b–d) fully-processed CdS networks with ED stages of (b) 5, (c) 10, and (d) 15 min.

Figure 4a illustrates the optical absorption properties of the samples. Compared to their as-calcinated counterpart, the fully-processed structures are clearly seen to exhibit a sharper absorption edge and higher absorption intensity values at wavelengths below 500 nm, with this trend becoming stronger with ED time. The increasingly sharper absorption edge might arise from a narrower size distribution of the nanoparticles,[46] while the higher absorption intensity resulted from the thicker network wall and larger crystal sizes

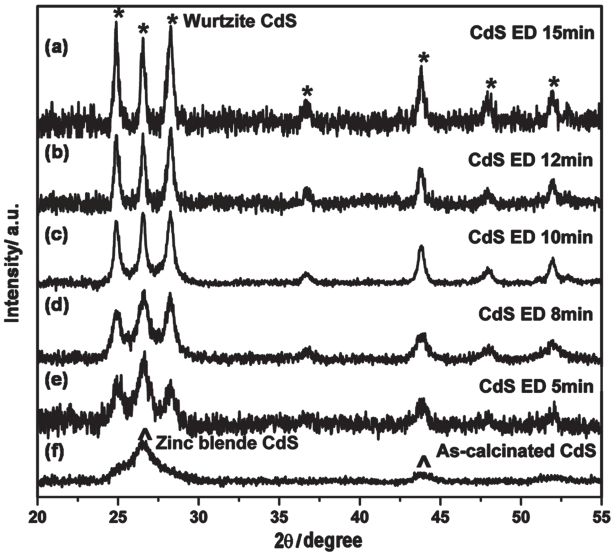

Figure 3. XRD patterns of (a–e) fully-processed structures with ED times of (a) 15, (b) 12, (c) 10, (d) 8 and (e) 5 min, and (f) as-calcinated CdS inverse opal structure.

observed in the fully-processed samples. Both these characteristics are believed to be beneficial for the light harvesting in SCs. Moreover, the absorption edge of the fully-processed structures is seen to blue-shift compared to that of the as-calcinated structure, which is probably related to the elimination of structure defects, such as twinning or stacking faults, caused by the annealing.[39]

Photoluminescent (PL) spectra of the samples are presented in Figure 4b. The as-calcinated sample is seen to have its emission peak centered at 2.38 eV, while those of the fully processed samples are located at 2.34 eV. All the PL peaks can be ascribed to the near-band-edge (NBE) emission of CdS,[47] because the bulk CdS possesses a band gap of 2.4 eV. The slight PL blue-shift of the as-calcinated sample could arise from the quantum confinement effect due to the small particle size (~4 nm). Importantly, the PL intensity increases with CdS ED time. This indicates that non-irradiative defects could be eliminated during ED and subsequent annealing, supporting the conclusions drawn from the absorption results shown in Figure 4a.

Figure 4c displays the photocurrent density-voltage characteristics of the samples, thus comparing their photovoltaic performance. The as-calcinated structure is seen to exhibit the lowest short-circuit photocurrent density (J_{SC}) (also see Table 1), while the samples ED-treated for 5, 8 and 10 min (and then annealed) demonstrated gradually increasing values of J_{SC} and open-circuit voltage (V_{OC}). Under optimal conditions (ED time of 10 min), they reached the values of 6.58 mA/cm^2 and 0.76 V, respectively, and an overall conversion efficiency (η) of 2% (as seen in Figure 4c and Table 1). To our best knowledge, this value is the highest ever reported for CdS-nanostructure based SCs (and measured with a two-electrode system). Moreover, the V_{OC} of 0.76 V is close to the theoretical energy difference between the Fermi level of CdS and the Nernst potential of the redox couple in the polyiodide electrolyte.[48] As seen from Table 1, further CdS ED caused a deterioration of J_{SC}, V_{OC} and η of the fully-processed samples. In addition, as seen in Figure S6 for the fully-processed sample ED-treated for 10 min, the corresponding photocurrent response of CdS network electrodes to on/off cycles demonstrated steady photocurrent generation.

The incident photon-to-electron conversion efficiency (IPCE) curves for different samples are shown in Figure 4d. The curves for both the as-calcinated and fully-processed CdS networks are seen to have an onset of photocurrent at 540 nm, confirming that the photoresponse arises from the band gap excitation of CdS nanocrystals. Moreover, the as-calcinated structure exhibits the lowest photocurrent generation efficiency, while the sample ED-treated for 10 min achieves the highest value of 58.5%, which agrees well with the highest J_{SC} value demonstrated by this sample (see Figure 4c).

To understand better the difference in sample performance observed in Figure 4c, electrochemical impedance spectroscopy (EIS) was employed under dark conditions and at different negative-bias voltages. **Figure 5**a displays the results taken at –0.15 V, while Figure 5b is the enlargement of the high-frequency range of the spectra in panel (a), showing straight lines normally indicative of the Warburg behavior characteristic of a transmission line.[49–52] Therefore, the corresponding model, previously developed by Bisquert *et al.*[49–52] (see the equivalent circuit in Figure 5c and details in the Supporting Information), was used to fit the results.

Fitting the EIS results to the transmission line model allowed us to obtain such important photoanode parameters as the

Table 1. Wall thickness, average crystal size determined from XRD, and performance characteristics of the as-calcinated and fully-processed structures with different ED times.

Sample	Wall thickness [nm]	Phase structure	Grain size [nm]	V_{OC} [V]	J_{SC} [mA/cm^2]	FF	η [%]
As-calcinated	17	Zinc-blende	3.5	0.68	3.07	0.41	0.86
		Wurtzite	4.3				
Fully-processed with 5 min ED	33	Wurtzite	10	0.71	4.05	0.48	1.38
Fully-processed with 8min ED	42	Wurtzite	15	0.74	5.06	0.43	1.61
Fully-processed with 10 min ED	50	Wurtzite	25	0.76	6.58	0.40	2.00
Fully-processed with 12 min ED	68	Wurtzite	28	0.63	4.92	0.42	1.30
Fully-processed with 15 min ED	85	Wurtzite	29	0.59	4.63	0.42	1.15

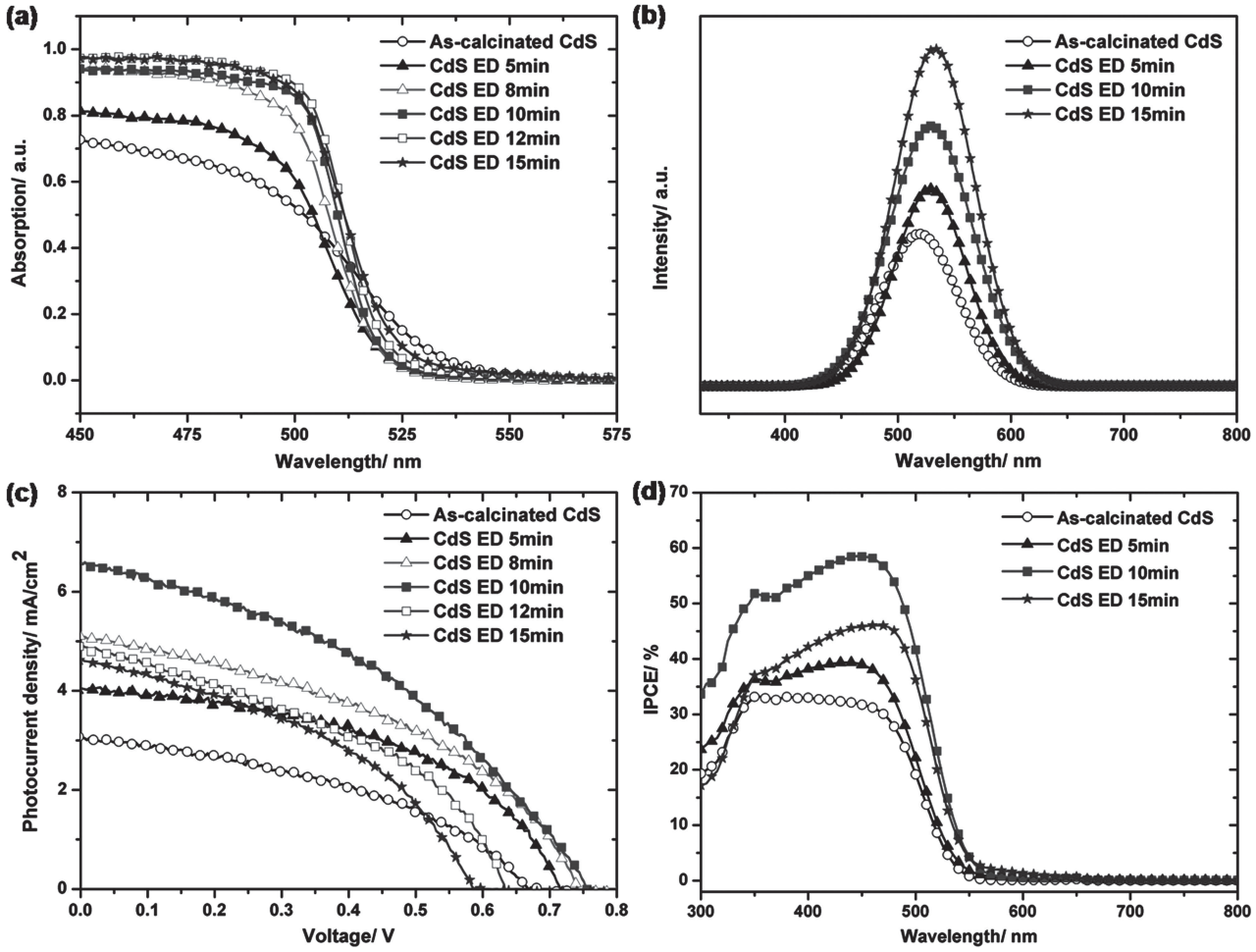

Figure 4. (a) UV–vis absorption spectra, (b) PL spectra, (c) current–voltage performance under illumination of one sun (AM1.5, 100 mW/cm^2) and (d) Incident photon to current conversion efficiency (IPCE) curves of the as-calcinated and fully-processed structures (with different ED times).

electron transport resistance of the CdS backbone (R_t) and the recombination resistance at the CdS/electrolyte interface (R_{ct}). As seen in Figure 5d, the as-calcinated structure demonstrated high R_t values above 10^3 Ω cm^2, which were remarkably reduced after the ED and annealing treatment. The high R_t values of the as-calcinated structure can be ascribed to its smaller CdS nanocrystals (about 4 nm in size, see Table 1) and to a large number of interfaces between them, while the latter are prone to electron trapping and scattering.[34,53] The network walls of the fully-processed structures were thickened and their grains became significantly larger. This significantly reduced the transport resistance of the material. As seen in Figure S7, the R_t values of the fully-processed structure with ED treatment for 15 min were even slightly lower than those of CdS-sensitized ZnO single-crystal nanowires (the latter being known as a superior material for electron transport[4]).

Figure 5e exhibits that the sample ED-treated for 10 min demonstrated the largest R_{ct} values, while the recombination resistance of the as-calcinated structure was always the lowest among all the samples. This could be also ascribed to the difference in the sample microstructures. The porous walls in the as-calcinated CdS network are very likely to intensify charge recombination at the CdS/electrolyte interface and to lower the R_{ct} value. Since during the ED and annealing treatments the nanopores were filled up and the grains grew up much larger, this dramatically reduced the solid/liquid interface and inter-grain areas. As a result, the probability of charge recombination was lowered, while the recombination resistance (Figure 5e) was increased and the electron lifetime (Figure 5f) expanded, thus leading to the improved electron collection efficiency of the device.[54,55] However, excessively long CdS ED (i.e., for over 10 min) was found to cause lower R_{ct} values (see Figure 5e), which can be attributed to a further increase in wall thickness but only a slight increase in grain size, as seen in Table 1. This resulted in more inter-grain boundaries which can act as recombination centers for photo-induced carriers. In this case, the recombination was believed to proceed preferentially within the nanocrystals.

Based on the above, we clarify the role of each step in the presented process as follows. The co-deposition and calcinations produced a 3D CdS framework with an inverse opal structure. However, the transport resistance of the material

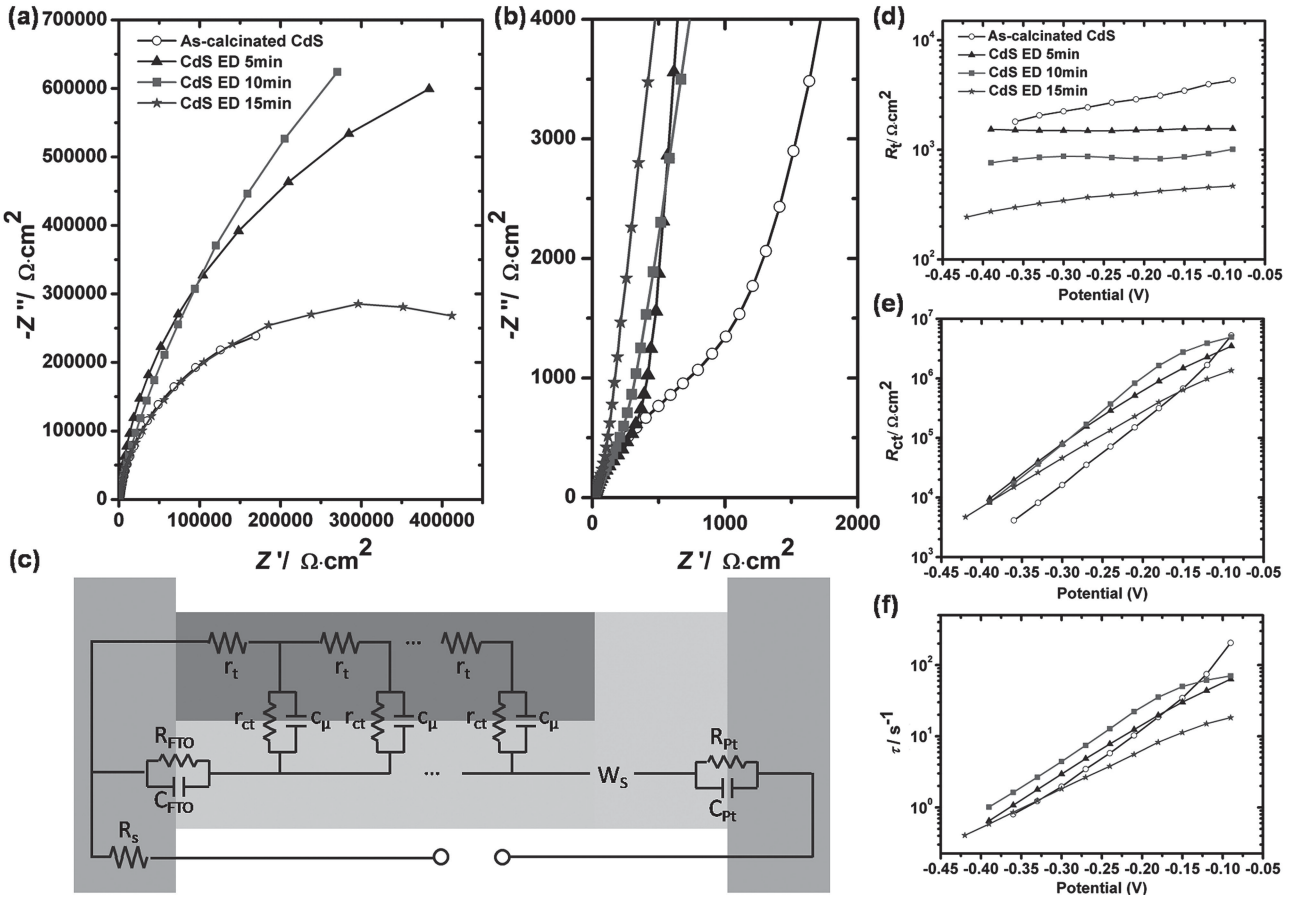

Figure 5. Results of EIS measurements of the as-calcinated (squares) and fully-processed (triangles) 3D CdS structures. (a) EIS spectra measured at a bias voltage of –0.15 V under dark conditions, (b) enlargement of the high-frequency range in (a). (c) Equivalent fitting circuit of the transmission line model used in this study. (d) Electron transport resistance (R_t), (e) recombination resistance (R_{ct}) and (f) electron lifetime (τ) of the samples as a function of applied bias voltage.

was relatively high while the recombination resistance was low due to its porous walls made of ultrafine nanocrystals. Moreover, its thin walls could not absorb the incident light efficiently and had quite many defects. As a result, the SC based on the as-calcinated structure could only demonstrate a conversion efficiency of ~0.86%, similar to other inverse opal structures.[28,29] The subsequent ED and annealing treatments eliminated the structural defects and increased the wall thickness and crystal size. This largely improved its light harvesting, reduced the transport resistance, enhanced the recombination resistance, as well as expanded electron lifetime. As a result, the SCs based on the fully-processed structures showed much improved J_{SC}, V_{OC}, and η values. Specifically, the sample ED-treated for 10 min was found to demonstrate an appropriate wall thickness and grain size, which resulted in the largest recombination resistance, the longest electron lifetime, the highest IPCE, and eventually the best power conversion performance. However, excessive ED treatment, e.g. 15 min ED, caused undue wall thickness of the porous structure without obvious improvement on grain size, which deteriorated the charge separation and then overall performance of the material. Therefore, post-treatments under optimum conditions are necessary to achieve high power-conversion efficiency.

Since CdSe has a narrower band-gap and can form a type-II semiconductor hetero-junction with CdS, we attempted the deposition of an additional CdSe layer onto fully processed CdS inverse opals (with CdS ED time of 10 min) to improve further the light absorption and promote the charge separation of the structure. Characterization details of the final structure are given in Figure S8. As seen in **Figure 6** and **Table 2**, with the optimized CdSe deposition time of 120 s, the J_{SC} value could reach 11.68 mA/cm^2, which is almost 1.8 times larger than the best value previously shown in Figure 4c. The increased value of the filled factor (FF) and photoresponse of IPCE (Figure S9) implies that the energy band structure alignment between the CdS backbone and CdSe layer definitely enhanced both charge separation and drive electron injection from CdSe to CdS in the final product.[56,57] Although the V_{OC} decreased somewhat after the CdSe deposition due to its lower Fermi energy level (compare Figures 4c and 6), the overall conversion efficiency of the CdSe/CdS system was raised up to 2.47%.

Several works have previously reported on the application of CdS or CdSe semiconductor nanocrystals with narrow

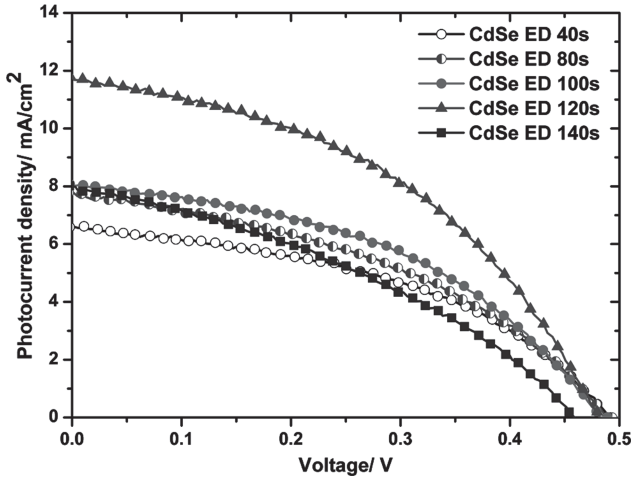

Figure 6. Current–voltage curves of optimal fully-processed CdS structures (with CdS ED time of 10 min) additionally coated with CdSe for different times.

Table 2. Performance of fully-processed CdS structures (with CdS ED time of 10 min) additionally coated with CdSe for different times.

Sample	V_{OC} [V]	J_{SC} [mA/cm^2]	FF	η [%]
ED CdSe 40s	0.49	6.79	0.43	1.43
ED CdSe 80s	0.50	7.78	0.41	1.61
ED CdSe 100s	0.49	8.07	0.44	1.73
ED CdSe 120s	0.48	11.68	0.44	2.47
ED CdSe 140s	0.46	7.98	0.36	1.33

band gaps as both light harvesters and carrier conductors in SCs.[2,58–60] As seen in **Table 3**, where the results are summarized, all the previous devices demonstrated relatively low FF values, which can be ascribed to their poor conductivity and severe charge recombination. In this regard, the SCs with 3D CdS networks described in the present work achieved superior performance levels (in terms of their J_{SC}, V_{OC} and FF). It is believed that even higher conversion efficiencies can be achieved through a further optimization of the above structures, e.g., introducing a hole blocking layer between the FTO and CdS network, or adopting more efficient light harvesters, electrolytes and counter electrodes.

3. Conclusions

3D inverse-opal structures of CdS were constructed via a novel route based on co-assembling followed by calcination. The electrical conductivity of the as-prepared networks was dramatically improved by a subsequent CdS electrodeposition step combined with annealing, which resulted in thicker walls and larger grains in the material. Compared to previously reported counterparts, the fully processed structures exhibited a higher efficiency of light harvesting, larger interface area for charge separation and higher conductivity for carrier transport. They were applied as photoanodes in solar cells and achieved a conversion efficiency of 2.00% (100 mW/cm^2), which is the highest value ever reported for photochemical cells based on CdS nanocrystals. The highly conductive 3D networks described in this study look very promising for the further development of solid-sate solar cells, for example, those of p–n junction type. Their high carrier-transport and charge-separation properties are of high demand for photovoltaic applications.

4. Experimental Section

Synthesis of Water-Stable CdS Quantum Dots: CdS quantum dots (QDs) were synthesized following the previously reported recipe.[61] First, 0.1 mol/L $CdCl_2$ and 0.1 mol/L thioacetamide solutions were prepared. Second, 50 mL of $CdCl_2$ was heated to 80 °C, then 869 µL of thioglycolic acid was added into the solution whose pH value was adjusted to 8 by adding NaOH. After that, 50 mL of thioacetamide solution was added, and the resulting solution was kept at 80 °C under stirring for 2 h. When the reaction was completed, ethanol was added to precipitate CdS QDs, which were then separated by centrifugation. The final precipitated CdS QDs were dispersed in distilled water, where their concentration was kept at 3.14 wt%. The resulting CdS QDs dispersion was transparent with a light-yellow color, indicating a good stability of CdS QDs in water.

Preparation of the As-Calcinated CdS Inverse Opal Structures: As-received monodispersed PS spheres with the size of 300 nm were dispersed in distilled water to form a 6% solution. 0.5 mL of the dispersion and 0.75 mL of CdS QD dispersion were added into a beaker containing 20 mL of distilled water to form a uniform mixture. Then, clean FTO substrates were inserted vertically into the mixture. The beaker was maintained in a vacuum oven heated at 60 °C for 24 h. Upon solvent (water) evaporation, the PS spheres and CdS QDs were co-assembled on the FTO substrates. Finally, the FTO substrates were annealed at 400 °C in air for 1 h to remove the PS templates. The thickness of as-prepared CdS inverse opals was approximately 2.6 µm. To prepare CdS inverse opals with the thickness of 1.0, 1.7, and 3.8 µm, the volume of PS dispersion was taken as 0.19, 0.33 and 0.73 mL, respectively, while the volume of the CdS QD dipsersion was 0.29, 0.49, and 1.10 mL, respectively. Compared with the conventional two-step process typically used for inverse opal preparation, which involves

Table 3. Performance characteristics of previously reported photochemical cells with narrow-band-gap semiconductor nanocrystals acting both as light harvesting and transporting materials.

Light harvesting and transporting materials	V_{OC} [V]	J_{SC} [mA/cm^2]	FF	η [%]	Thickness [µm]	Electrolyte	Reference
CdSe nanowire/quantum dots	0.58	0.06	0.29	0.01	–	Na_2S electrolyte	Yu et al.[58]
CdSe nanoparticles	0.37	12.95	0.26	1.25	0.1	Na_2S/S electrolyte	Lai and Chou[59]
CdS nanocrystals	0.62	4.46	0.27	0.75	2	Iodide electrolyte	Ling et al.[60]
3D CdS networks	0.76	6.58	0.40	2.00	2.6	Iodide electrolyte	Present work
3D CdS/CdSe networks	0.48	11.68	0.44	2.47	2.6	Iodide electrolyte	Present work

the assembly of a solid template and then infiltration of a precursor solution,[15–19] the co-deposition approach skips the latter stage. As a result, this permits to evade the possibility of non-uniform distribution of a precursor solution and template damages, which usually emerge in the conventional process.[15–19]

Electrodeposition and Annealing Treatments of CdS Inverse Opals: The electrodeposition of additional CdS layers was performed at a current density of 0.5 mA/cm^2 in a two-electrode cell where the FTO substrate (coated with CdS inversed opals) and Pt were used as the working and the counter electrodes, respectively. The electrolyte was a dimethyl sulfoxide solution containing 0.055 M $CdCl_2$ and 0.19 M sulfur (the electrolyte temperature being kept at 110 °C). The as-deposited CdS networks were then annealed at 400 °C (for 1 h) for crystallization. As shown in Supplementary Information Figure S3 and Table S2, the grain size of the CdS networks could be remarkably enlarged with annealing temperature. Nevertheless, annealing at temperatures above 400 °C resulted in the formation of CdO, which worsened the light harvesting and electronic properties of the CdS structures.[59] Therefore, the annealing temperature was set as 400 °C.[62]

Solar Cell Assembly: The FTO substrate covered with fully-processed (i.e., as-calcinated and then electrodeposited with additional CdS and annealed) CdS networks was sealed with a thin transparent hot-melt Surlyn with an active area of 0.24 cm^2 to the counter electrode (Pt on FTO glass) A metallic mask with a window of slightly larger than 0.24 cm^2 was clipped on the CdS side (Figure S10) to avoid the aperture effect.[63] An iodide-based electrolyte, consisting of 0.5 M LiI, 0.05 M I_2, 0.3 M tert-butylpyridine, and 0.3 M tetra-butylammonium iodide in acetonitrile, was injected into the inner electrode space from the counter electrode side through a predrilled hole.

Characterization: SEM was performed on a Hitachi S-4800 scanning electron microscope operated at 5 kV. TEM was performed using a Technai G2 F20 with a field emission gun operated at 200 kV. XRD analysis was carried out using a Bruker D/max 2500 v/pc diffractometer. The absorption spectra of the samples were examined using a Hitachi 3010 UV–vis absorption spectrometer. Photoluminescent (PL) analyses were performed with a Hitachi F-4500 fluorescence spectrometer at room temperature using 310 nm excitation wavelength. Photocurrent density–voltage (*J–V*) curves were measured under an illumination of a solar simulator (Sciencetech, SS150) at one sun (AM 1.5, 100 mW/cm^2). A Keithley 2611 digital source meter was used to record the *J–V* curves. IPCE spectra were measured with a tungsten quartz halogen light source, mono-chromator, filters, reflective optics to provide monochromatic light, mechanical chopper to modulate the light, and transition impedance amplifier to provide the test device signal to the digital signal processing equipment. Electrochemical impedance spectroscopy (EIS) data of the cells were collected by using a Versastat 3 Potentiostats-Electrochemistry workstation in the frequency range from 0.1 Hz to 100 kHz under forward bias from –0.05 to –0.42 V.

Supporting Information

Supporting Information is available from the Wiley Online Library or from the author.

Acknowledgements

This work was supported by the Natural Science Foundation of China (Nos. 51171127, 51102176 and 11272229), Natural Science Foundation of Tianjin City (Nos. 11ZCKFGX01300, 11JCYBJC02000 and 09JCZDJC22600) and Seed Foundation of Tianjin University.

Received: February 27, 2013
Revised: June 3, 2013
Published online: August 21, 2013

[1] M. Grätzel, *Nature* **2001**, *414*, 338.
[2] W. U. Huynh, J. J. Dittmer, A. P. Alivisatos, *Science* **2002**, *295*, 2425.
[3] B. M. Kayes, H. A. Atwater, N. S. Lewis, *J. Appl. Phys.* **2005**, *97*, 114302.
[4] M. Law, L. E. Greene, J. C. Johnson, R. Saykally, P. D. Yang, *Nat. Mater.* **2005**, *4*, 455.
[5] N. S. Lewis, *Science* **2007**, *315*, 798.
[6] A. Luque, A. Marti, A. J. Nozik, *MRS Bull.* **2007**, *32*, 236.
[7] Y. Zhang, L.-W. Wang, A. Mascarenhas, *Nano Lett.* **2007**, *7*, 1264.
[8] G. Hodes, *J. Phys. Chem. C* **2008**, *112*, 17778.
[9] P. V. Kamat, *J. Phys. Chem. C* **2008**, *112*, 18737.
[10] A. J. Nozik, *Physica E* **2002**, *14*, 115.
[11] J. B. Sambur, T. Novet, B. A. Parkinson, *Science* **2010**, *330*, 63.
[12] R. D. Schaller, V. I. Klimov, *Phys. Rev. Lett.* **2004**, *92*, 186601.
[13] O. E. Semonin, J. M. Luther, S. Choi, H.-Y. Chen, J. Gao, A. J. Nozik, M. C. Beard, *Science* **2011**, *334*, 1530.
[14] Z. Fan, H. Razavi, J.-w. Do, A. Moriwaki, O. Ergen, Y.-L. Chueh, P. W. Leu, J. C. Ho, T. Takahashi, L. A. Reichertz, S. Neale, K. Yu, M. Wu, J. W. Ager, A. Javey, *Nat. Mater.* **2009**, *8*, 648.
[15] B. T. Holland, C. F. Blanford, A. Stein, *Science* **1998**, *281*, 538.
[16] O. D. Velev, A. M. Lenhoff, *Curr. Opin. Colloid Interface Sci.* **2000**, *5*, 56.
[17] Y. N. Xia, B. Gates, Y. D. Yin, Y. Lu, *Adv. Mater.* **2000**, *12*, 693.
[18] X. S. Zhao, F. B. Su, Q. F. Yan, W. P. Guo, X. Y. Bao, L. Lv, Z. C. Zhou, *J. Mater. Chem.* **2006**, *16*, 637.
[19] B. Hatton, L. Mishchenko, S. Davis, K. H. Sandhage, J. Aizenberg, *Proc. Natl. Acad. Sci. USA* **2010**, *107*, 10354.
[20] B. Mandlmeier, J. M. Szeifert, D. Fattakhova-Rohlfing, H. Amenitsch, T. Bein, *J. Am. Chem. Soc.* **2011**, *133*, 17274.
[21] S. Nishimura, N. Abrams, B. A. Lewis, L. I. Halaoui, T. E. Mallouk, K. D. Benkstein, J. van de Lagemaat, A. J. Frank, *J. Am. Chem. Soc.* **2003**, *125*, 6306.
[22] S. Guldin, S. Huttner, M. Kolle, M. E. Welland, P. Mueller-Buschbaum, R. H. Friend, U. Steiner, N. Tetreault, *Nano Lett.* **2010**, *10*, 2303.
[23] T. Suezaki, P. G. O'Brien, J. I. L. Chen, E. Loso, N. P. Kherani, G. A. Ozin, *Adv. Mater.* **2009**, *21*, 559.
[24] E. S. Kwak, W. Lee, N.-G. Park, J. Kim, H. Lee, *Adv. Funct. Mater.* **2009**, *19*, 1093.
[25] L. Liu, S. K. Karuturi, L. T. Su, A. I. Y. Tok, *Energ. Environ. Sci.* **2011**, *4*, 209.
[26] A. Mihi, C. Zhang, P. V. Braun, *Angew. Chem. Int. Ed.* **2011**, *50*, 5711.
[27] L. J. Diguna, Q. Shen, J. Kobayashi, T. Toyoda, *Appl. Phys. Lett.* **2007**, *91*, 23116.
[28] A. Esmanski, G. A. Ozin, *Adv. Funct. Mater.* **2009**, *19*, 1999.
[29] H. Zhang, P. V. Braun, *Nano Lett.* **2012**, *12*, 2778.
[30] C. V. Subban, I. C. Smith, F. J. DiSalvo, *Small* **2012**, *8*, 2824.
[31] J.-H. Choi, S.-H. Kwon, Y.-K. Jeong, I. Kim, K.-H. Kim, *J. Electrochem. Soc.* **2011**, *158*, B749.
[32] C. Cheng, S. K. Karuturi, L. Liu, J. Liu, H. Li, L. T. Su, A. I. Y. Tok, H. J. Fan, *Small* **2012**, *8*, 37.
[33] W.-T. Sun, Y. Yu, H.-Y. Pan, X.-F. Gao, Q. Chen, L.-M. Peng, *J. Am. Chem. Soc.* **2008**, *130*, 1124.
[34] J. Jasieniak, B. I. MacDonald, S. E. Watkins, P. Mulvaney, *Nano Lett.* **2011**, *11*, 2856.
[35] X.-Y. Chen, T. Ling, X.-W. Du, *Nanoscale* **2012**, *4*, 5602.
[36] T. Ling, M. Wu, X. Du, *Semicond. Sci. Technol.* **2012**, *27*, 055017.
[37] P. V. Braun, P. Wiltzius, *Nature* **1999**, *402*, 603.
[38] P. Braun, P. Wiltzius, *Adv. Mater.* **2001**, *13*, 482.
[39] Y. C. Lee, T. J. Kuo, C. J. Hsu, Y. W. Su, C. C. Chen, *Langmuir* **2002**, *18*, 9942.
[40] A. Blanco, H. Miguez, F. Meseguer, C. Lopez, F. Lopez-Tejeira, J. Sanchez-Dehesa, *Appl. Phys. Lett.* **2001**, *78*, 3181.

[41] F. Meseguer, A. Blanco, H. Miguez, F. Garcia-Santamaria, M. Ibisate, C. Lopez, *Colloid. Surf. A* **2002**, *202*, 281.
[42] A. N. Goldstein, C. M. Echer, A. P. Alivisatos, *Science* **1992**, *256*, 1425.
[43] Y. A. Vlasov, N. Yao, D. J. Norris, *Adv. Mater.* **1999**, *11*, 165.
[44] R. Banerjee, R. Jayakrishnan, P. Ayyub, *J. Phys. Condens. Matter* **2000**, *12*, 10647.
[45] K.-T. Yong, Y. Sahoo, M. T. Swihart, P. N. Prasad, *J. Phys. Chem. C* **2007**, *111*, 2447.
[46] S. Datta, K. L. Narasimhan, *Phys. Rev. B* **1999**, *60*, 8246.
[47] J. Aguilar-Hernández, J. Sastre-Hernández, N. Ximello-Quiebras, R. Mendoza-Pérez, O. Vigil-Galán, G. Contreras-Puente, M. Cárdenas-Garcıa, *Thin Solid Films* **2006**, *511/512*, 143.
[48] M. Grätzel, *Nature* **2001**, *414*, 338.
[49] J. Bisquert, *J. Phys. Chem. B* **2002**, *106*, 325.
[50] F. Fabregat-Santiago, J. Bisquert, G. Garcia-Belmonte, G. Boschloo, A. Hagfeldt, *Sol. Energy Mater. Sol. Cells* **2005**, *87*, 117.
[51] F. Fabregat-Santiago, J. Bisquert, E. Palomares, L. Otero, D. Kuang, S. M. Zakeeruddin, M. Gratzel, *J. Phys. Chem. C* **2007**, *111*, 6550.
[52] F. Fabregat-Santiago, G. Garcia-Belmonte, I. Mora-Sero, J. Bisquert, *Phys. Chem. Chem. Phys.* **2011**, *13*, 9083.
[53] R. Tena-Zaera, A. Katty, S. Bastide, C. Levy-Clement, *Chem. Mater.* **2007**, *19*, 1626.
[54] H. Lee, M. Wang, P. Chen, D. R. Gamelin, S. M. Zakeeruddin, M. Graetzel, M. K. Nazeeruddin, *Nano Lett.* **2009**, *9*, 4221.
[55] H. Han, P. Sudhagar, T. Song, Y. Jeon, I. Mora-Seró, F. Fabregat-Santiago, J. Bisquert, Y. S. Kang, U. Paik, *Chem. Commun.* **2013**, *49*, 2810.
[56] Y.-L. Lee, Y.-S. Lo, *Adv. Funct. Mater.* **2009**, *19*, 604.
[57] Y.-L. Lee, C.-F. Chi, S.-Y. Liau, *Chem. Mater.* **2010**, *22*, 922.
[58] Y. Yu, P. V. Kamat, M. Kuno, *Adv. Funct. Mater.* **2010**, *20*, 1464.
[59] C.-H. Lai, P.-T. Chou, *Chem. Commun.* **2011**, *47*, 3448.
[60] T. Ling, M.-K. Wu, K.-Y. Niu, J. Yang, Z.-M. Gao, J. Sun, X.-W. Du, *J. Mater. Chem.* **2011**, *21*, 2883.
[61] H. Peng, L. Zhang, C. Soeller, J. Travas-Sejdic, *J. Lumin.* **2007**, *127*, 721.
[62] N.-H. Kim, S.-H. Ryu, H.-S. Noh, W.-S. Lee, *Mater. Sci. Semicond. Proc.* **2012**, *15*, 125.
[63] S. Ito, M. K. Nazeeruddin, P. Liska, P. Comte, R. Charvet, P. Pechy, M. Jirousek, A. Kay, S. M. Zakeeruddin, M. Graetzel, *Prog. Photovoltaics* **2006**, *14*, 589.